

Robustness of Optimal Energy Thresholds in Photon-counting Spectral CT

Yifan Zheng^{1,2,5}, Moa Yveborg³, Fredrik Grönberg¹, Cheng Xu^{1,3}, Qianqian Su², Mats Danielsson^{1,3} and Mats Persson⁴

¹ Department of Physics, Royal Institute of Technology, Albanova University Center, SE-106 91 Stockholm, Sweden

² Key Laboratory of Particle and Radiation Imaging (Ministry of Education) and Department of Engineering Physics, Tsinghua University, Beijing 100084, China

³ Prismatic Sensors AB, Roslagstullsbacken 21, Stockholm 106 91, Sweden

⁴ Departments of Bioengineering and Radiology, Stanford University, Stanford 94305, California, USA

⁵ Author to whom any correspondence should be addressed

E-mail: yifanzhe@kth.se

February 2018

Abstract. An important question when developing photon-counting detectors for computed tomography is how to select energy thresholds. In this work thresholds are optimized by maximizing signal-difference-to-noise ratio squared (SDNR²) in a silicon-strip detector and a cadmium zinc telluride (CZT) detector, factoring in pileup in both detectors and charge sharing in the CZT detector. To investigate to what extent one single set of thresholds could be applied in various imaging tasks, the robustness of optimal thresholds with 2 to 8 bins is examined with the variation of anatomies and tissues. In contrast to previous studies, the optimal threshold locations don't always increase with increasing anatomies if pileup is included. Optimizing the thresholds for a 30 cm phantom yields near-optimal SDNR² regardless of anatomies and tissues in both detectors. Fixing that set of thresholds and including pileup, with 2 bins, up to 23% of SDNR² is lost; and with 6 to 8 bins, the loss of SDNR² is 5% in the silicon-strip detector and 8% in the CZT detector. Having more than 2 bins reduces the need for changing the thresholds depending on anatomies and tissues. Using around 6 bins may give near-optimal SDNR² without generating an unnecessarily large amount of data.

Keywords: photon counting, spectral CT, threshold optimization, silicon-strip detector, CZT detector

Submitted to: *Phys. Med. Biol.*

1. Introduction

Photon-counting spectral CT with multi-bins has several advantages over conventional energy-integrating CT, including better image quality (Schmidt 2009), lower radiation dose (Chen et al. 2015, Le et al. 2010), and K-edge imaging feasibility (Roessl & Proksa 2007). The signal-difference-to-noise ratio (SDNR) can be increased by up to 60% in photon-counting CT with the same radiation dose as conventional CT (Bornefalk & Danielsson 2010). K-edge imaging can help to better distinguish and quantitate contrast agents (Schlomka et al. 2008, Roessl & Proksa 2007).

Photon-counting spectral CT detects incident photons and sort them into specific energy bins according to the deposited energy. Conventionally, the first threshold is set higher than the noise floor of the detector and the other thresholds are placed either in uniform increment or on some certain values (Persson et al. 2014, Roessl & Proksa 2007). The placement of energy thresholds is important in improving image quality (Müllner et al. 2015). To yield the maximum SDNR² and reduce patient dose at the same time, the energy thresholds require to be optimized. Moreover, the thresholds are set before exposure and it is inconvenient to change them during the scan. So it is desirable to find one single set of thresholds that gives close to the optimal performance regardless of the variation of patient anatomies and tissue compositions. In previous studies, the placement of optimal thresholds was calculated (Wang et al. 2011, Wang & Pelc 2009, Wang & Pelc 2011) and increased with phantom thicknesses as a result of the beam hardening effect (Shikhaliyev 2009, Wang & Pelc 2009, Roessl & Proksa 2006, Roessl et al. 2011). Better image quality was yielded with some thresholds placed around the K-edge of contrast agent (Cormode et al. 2010, Müllner et al. 2015). When optimizing energy thresholds in a cadmium zinc telluride (CZT) detector with six bins, the 'close bracketing' effect was found where two optimal thresholds closely surround the K-edge of the contrast agent (Roessl et al. 2011, W. H. Press & Flannery n.d.). However, previous studies have not investigated to what extent one single set of energy thresholds could be applied in various imaging tasks; and the detectors in those studies were assumed to be ideal, neglecting pulse pileup, charge sharing or K-fluorescence. A precise detector response plays an important role in setting optimal thresholds in real applications (Roessl et al. 2011).

The purpose of this work is to investigate the robustness of optimal energy thresholds with respect to the variation of anatomies and tissues. The optimal energy thresholds are examined based on two types of promising photon-counting detectors: silicon-strip detectors and CZT detectors. The influences of pulse pileup on the optimal threshold placement and the robustness of optimal thresholds are also analyzed in both detector models. In Sec. 2, simulation setup and the optimization algorithm are described, with SDNR² used as a figure of merit (FOM) to evaluate threshold optimization. The results are reviewed in sections 3 and 4.

2. Materials and Methods

The placement of energy thresholds is optimized for a silicon-strip detector and a CZT detector separately. The X-ray beams after 0.8 mm thick beryllium and 6 mm thick aluminum filtration pass through a D cm thick water phantom with an embedded 1 cm thick imaging target and reach the detector. The source-to-detector distance is 1,000 mm. The X-ray spectrum is generated by a tube with tungsten anode at 11 degrees. The tube voltage is set to 120 kilovoltage peak (kVp) and the tube current is 500 mA. The acquisition time for each projection is 100 μ s (Prince & Links 2006). The total fluence rate at the detector is $2.0 \times 10^6 \text{ mm}^{-2}\text{s}^{-1}\text{mA}^{-1}$ (Persson et al. 2016). Photon counts scattered by the object are not taken into consideration by assuming a perfect anti-scatter grid.

The silicon-strip detector has a maximum of 8 bins and is applied in edge-on geometry with one edge towards incident X-rays (Bornefalk & Danielsson 2010, Persson et al. 2014, Xu et al. 2013, Liu et al. 2014, Liu et al. 2015, Liu et al. 2016). It has a 0.5 mm thick dead layer on the front edge and a 3 cm thick active absorption layer subdivided into nine depth segments, with lengths exponentially increased to ensure a uniform count rate in each segment (Liu et al. 2015). The pixel size of each detector element is $0.4 \times 0.5 \text{ mm}^2$ (Xu et al. 2013, Liu et al. 2014). The energy resolution is approximately 1.6 keV over all energies from measurement (Liu et al. 2014). To model pileup distortion in the silicon-strip detector, the nonparalyzable model is applied with a dead time of 35 ns (Liu et al. 2016, Knoll 2010). The model agrees with the measured data for relatively low levels of pileup (Liu et al. 2016). Photoelectric effect and Compton scattering are modeled in the detector response function (Bornefalk & Danielsson 2010). The charge sharing effect is neglected in the silicon-strip detector because charge sharing is around 3% in lower energy segments and is further reduced by the anticoincidence logic in the readout electronics (Xu et al. 2011, Persson et al. 2014, Ballabriga et al. 2013, Koenig et al. 2013).

The CZT detector is originated from J. P. Schlomka (Schlomka et al. 2008), and has a maximum of 6 bins and a pixel size of $0.5 \times 0.5 \text{ mm}^2$. The thickness of the CZT detector is 3 mm with a 0.02 mm dead layer. The dead time is 40 ns for pileup distortion by applying the nonparalyzable model. The energy resolution is given by $\sigma = a_1 + a_2 \cdot E$, where a_1 is 1.61 keV and a_2 is 0.025 (Schlomka et al. 2008). In the detector response function, two Gaussian peaks are included to simulate the photoelectric effect and K-fluorescence, with one at the incident energy and the other at the energy reduced by the K-fluorescence energy. A step-like function is also included as background to simulate the charge sharing effect (Schlomka et al. 2008).

Pulse pileup can generate a distorted spectrum due to the stochastic arrival of photons and the dead time of all photon-counting detectors. Overlapping pulses may be detected as a single count with a higher energy. To simulate pulse pileup in both detectors, the Kth-order pileup model is applied to obtain the output distorted spectrum (Wang et al. 2011), and the multinomial distribution replaces the Poisson nature of the

total detected counts in each bin (Wang et al. 2011). Charge sharing is a significant effect in the CZT detector and results in incomplete charge collection, double counting and degraded image quality. If an incoming photon with an actual energy E_0 interacts between two neighboring pixels, the deposited energy in one pixel should always be larger than $E_0/2$ as a result of charge sharing (Liu et al. 2014, Xu et al. 2013). We assume the spectral distribution of primary counts, i.e excluding charge-shared counts from neighboring pixels, is obtained by discarding the deposited energies below $E_0/2$.

SDNR² is evaluated as a FOM in examining the optimal thresholds and the robustness of optimal thresholds. We look at the beam incident on one single pixel to avoid considering noise correlations among pixels. Factoring in pulse pileup and charge sharing, and taking into account the optimal weighting factor (Barrett & Myers 2013, Bornefalk 2011), SDNR² in the projection-based energy weighting method is given by (Barrett & Myers 2013)

$$\text{SDNR}^2 = \Delta g^T (K^b + K^t)^{-1} \Delta g \quad (1)$$

where $\Delta g = g^b - g^t$ is the difference between background counts $g^b = (I_1^b, \dots, I_N^b)^T$ and target counts $g^t = (I_1^t, \dots, I_N^t)^T$; K^b and K^t are the covariance matrices of g^b and g^t respectively; and I_i is the expected count in bin B_i with pileup considered, ($i = 1, 2, \dots, N$). For the CZT detector, the charge sharing effect makes it more complicated to calculate SDNR² since the counts in adjacent pixels will be correlated. To avoid the need for modeling spatial noise correlations, the target is assumed to be small enough to cover only a single pixel so that the charge sharing counts in the target case come from the surrounding pixels which contain only background information. The background bin counts I_i^b are calculated by propagating the full background spectrum $f^{b,cs}$, including charge sharing counts, through the Kth-order pileup model. In the target case, I_i^t are calculated by propagating the spectrum $f_*^{t,cs} = f^{b,cs} + f^{t,ncs} - f^{b,ncs}$, through the Kth-order pileup model. $f_*^{t,cs}$ is the sum of the background spectrum and a difference spectrum caused by the insertion of the target, where the difference spectrum does not include charge sharing counts from neighboring pixels, since these pixels are unaffected by the target.

The optimal thresholds for a photon-counting spectral CT system are to maximize SDNR² in Eq. 1. To search for the optimal thresholds, the Global-Search method based on the interior-point algorithm implemented in MATLAB is used to find the multi-dimensional maximal SDNR². Local maximal SDNR² could be reached from various starting points generated through a scatter-search mechanism, where the largest local maximum is regarded as the global maximum. The corresponding thresholds are taken as the optimal thresholds. At the optimal SDNR², the difference of SDNR² over a small difference of thresholds is given by the Taylor series stopping at the second order derivative

$$\begin{aligned}
|\Delta \text{SDNR}^2| &= |\nabla \text{SDNR}^2(T)^T \Delta T + \frac{1}{2} \Delta T^T H(T) \Delta T + O(\Delta T^2)| \\
&= \left| \frac{1}{2} \Delta T^T P^T \Lambda P \Delta T \right| \\
&\leq \frac{1}{2} |\lambda|_{\max} \|u\|^2
\end{aligned} \tag{2}$$

where $T = (t_1, t_2, \dots, t_N)$ is the threshold placement vector; the derivative $\nabla \text{SDNR}^2(T) = 0$ at the optimal SDNR^2 ; $H(T) = P^T \Lambda P$ is the eigendecomposition of the Hessian matrix; and $P \Delta T = u$ is regarded as a new variable. When $|\Delta T|$ is 1 keV, $|u| = |\Delta T|$ since P is an orthogonal matrix. Thus $|\Delta \text{SDNR}^2|$ is less than $|\lambda|_{\max}/2$, where $|\lambda|_{\max}$ is the maximum absolute eigenvalue of Hessian matrix $H(T)$. Therefore, $|\lambda|_{\max}/2$ theoretically reflects the decrease of optimal SDNR^2 when the distance between the selected thresholds and the optimal thresholds, measured as the vector norm between the two sets of thresholds, is 1 keV.

Both SDNR^2 and $|\lambda|_{\max}$ are normalized by the corresponding ideal SDNR^2 by assuming bins are set in a step of 1 keV, and they are denoted as relative SDNR^2 and relative decrease of SDNR^2 respectively. For each imaging target and each number of bins, Global-Search is run 15 times, which is enough to obtain stable optimal thresholds in real practice. The first threshold in the silicon-strip detector is set to 5 keV to discard electronic noise (Bornefalk & Danielsson 2010). In the CZT detector, the placement of the first threshold is optimized.

3. Results

When the target is 10 mg/mL iodine and the phantom thickness is 15 cm and 50 cm respectively, the spectra with pileup in the silicon-strip detector and the CZT detector are shown in Fig. 1. With phantom thickness $D = 15$ cm, the fraction of the pileup counts above 120 kVp in Fig. 1a is about 1.0% in the silicon-strip detector and 12.8% in the CZT detector. In comparison, the fraction of pileup decreases to 0.01% in the silicon-strip detector and 0.5% in the CZT detector with a thicker phantom in Fig. 1b.

Apart from the iodine contrast agent, common targets could also be bone or tumor in clinical applications. To investigate the performance of various target materials in the threshold optimization, targets are set as 10 mg/ml iodine, bone or tumor respectively and the phantom thickness is kept 30 cm. Considering pileup in both detectors, figure 2 presents relative optimal SDNR^2 and the relative decrease of optimal SDNR^2 when the distance between the selected thresholds and the optimal thresholds is 1 keV, as a function of bin numbers and targets.

Phantom thickness is important to the optimal threshold placement. To investigate the dependence of optimal thresholds on phantom thickness, optimal thresholds with 2 to 8 bins are calculated when the target is 10 mg/mL iodine and the phantom thickness is changed from 15 cm to 30 cm and 50 cm respectively. The optimal thresholds for

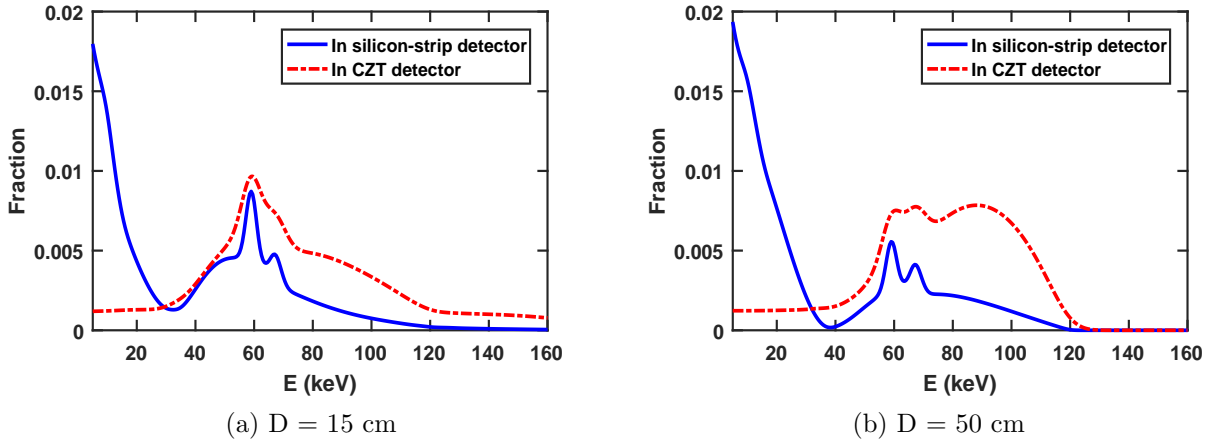


Figure 1: Spectra of 10 mg/ml iodine in the silicon-strip detector and the CZT detector considering pileup. The phantom thickness is (a) 15 cm and (b) 50 cm respectively.

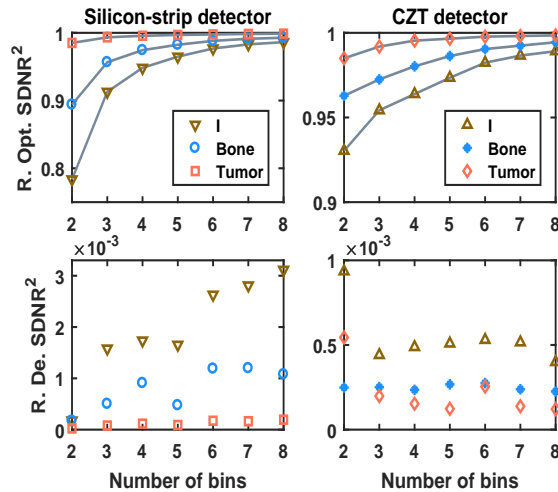


Figure 2: Relative optimal SDNR^2 and relative decrease of optimal SDNR^2 as a function of bin numbers in the silicon-strip detector and the CZT detector when considering pileup. The relative decrease of optimal SDNR^2 is given by $|\lambda|_{\max}/2$ in Eq. 2 normalized by the ideal SDNR^2 , when the distance between the selected thresholds and the optimal thresholds is 1 keV.

the silicon-strip detector and the CZT detector are shown in Fig. 3 and 4, factoring in pileup and no pileup separately.

To investigate the robustness of optimal thresholds and to what extent one single set of energy thresholds could be applied, SDNR^2 is examined with the variation of phantom thickness and target materials when the thresholds are fixed as the optimal thresholds for iodine. When the thresholds are fixed as the optimal thresholds for phantom 15 cm, 30 cm and 50 cm in Fig. 3 and 4, relative SDNR^2 as a function of phantom thickness

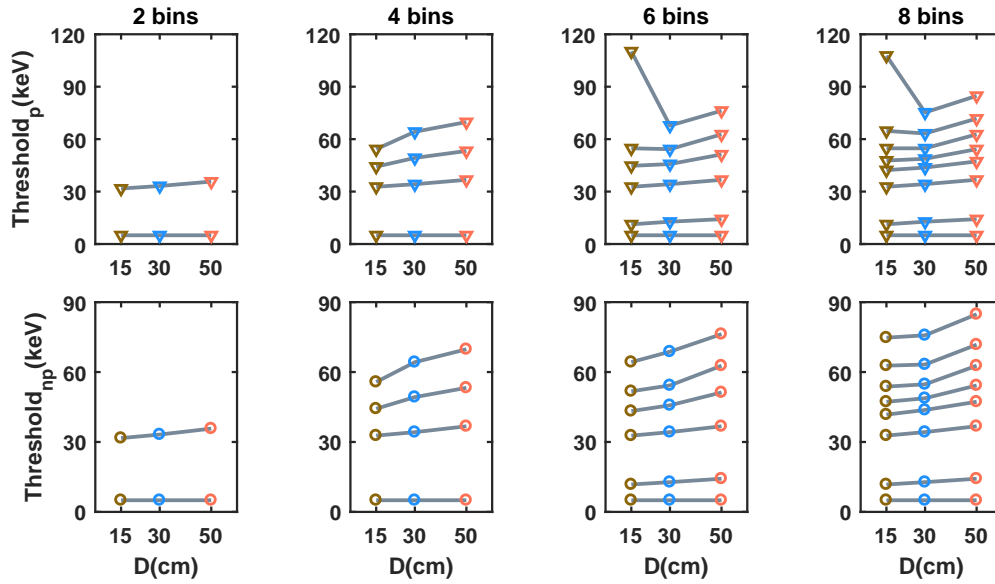


Figure 3: Optimal thresholds as a function of phantom thickness in the silicon-strip detector. The upper row considers pileup and the lower row neglects pileup.

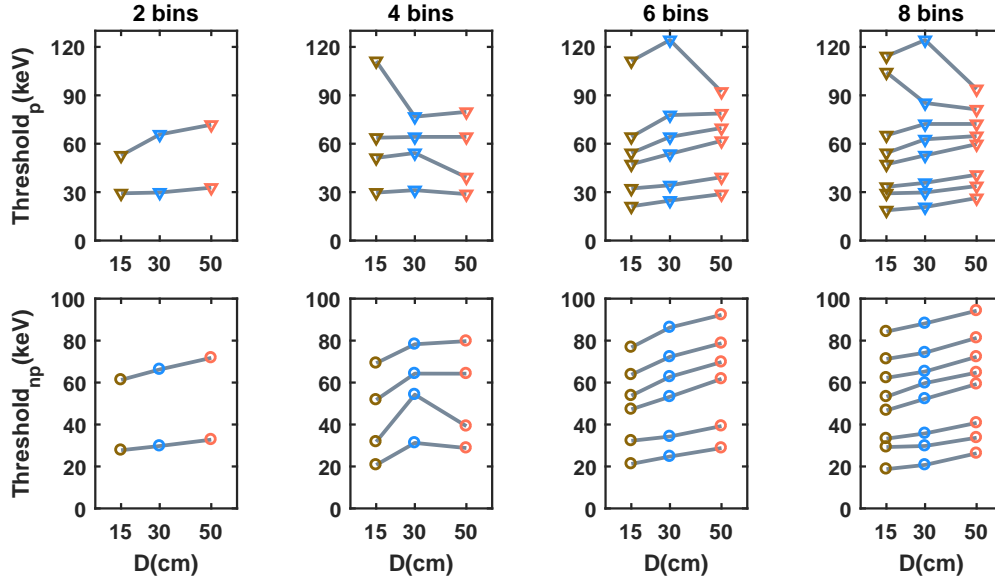


Figure 4: Optimal thresholds as a function of phantom thickness in the CZT detector. The upper row considers pileup and the lower row neglects pileup.

is shown in Fig. 5 in silicon-strip detector and in Fig. 6 in CZT detector. Then the thresholds are fixed as the optimal thresholds for phantom 30 cm only, relative SDNR² for a target of 1 mg/ml iodine, 10 mg/ml iodine, bone or tumor is shown in Fig. 7 and 8 with the variation of phantom thickness.

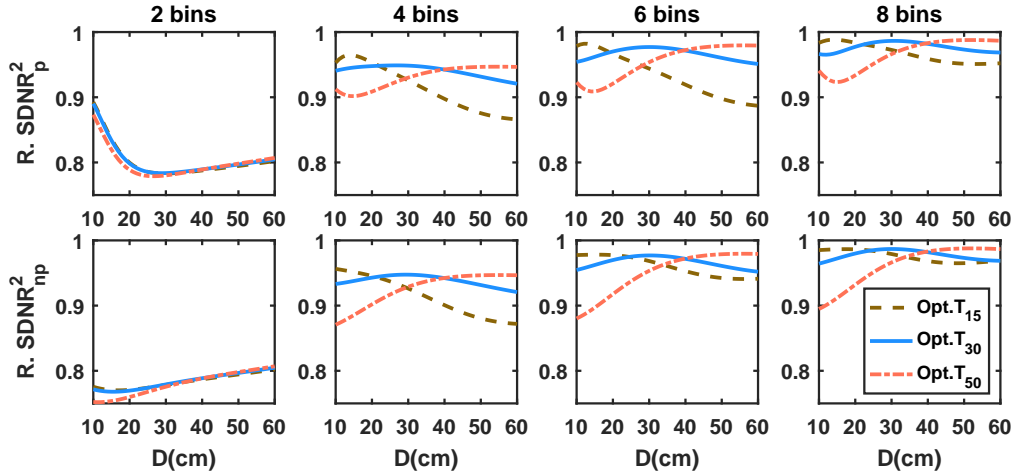


Figure 5: SDNR^2 as a function of phantom thickness in the silicon-strip detector when thresholds are fixed as the optimal thresholds for phantom 15 cm, 30 cm and 50 cm in Fig. 3. The upper row considers pileup and the lower row neglects pileup.

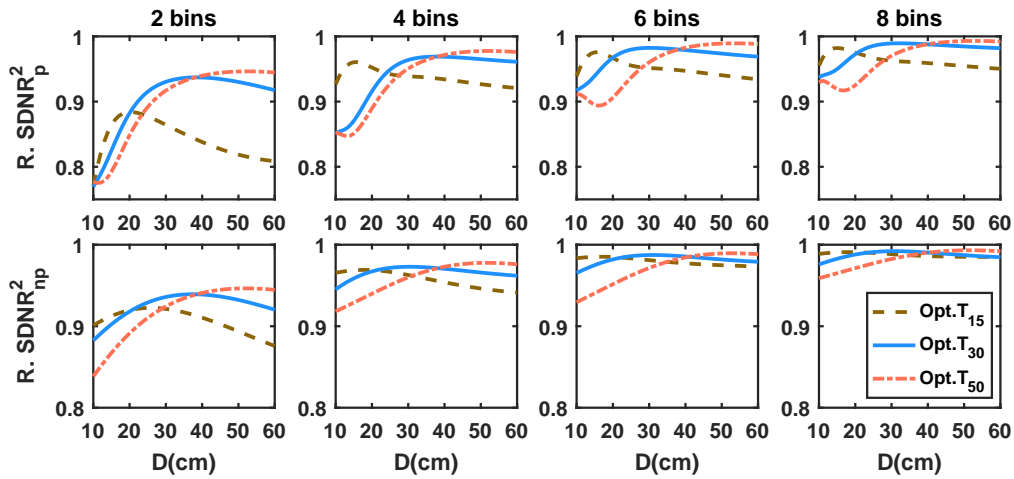


Figure 6: SDNR^2 as a function of phantom thickness in the CZT detector when thresholds are fixed as the optimal thresholds for phantom 15 cm, 30 cm and 50 cm in Fig. 4. The upper row considers pileup and the lower row neglects pileup.

4. Discussion

Optimal SDNR^2 and the placement of optimal thresholds are highly related to the detected spectrum, which is influenced by detectors, targets and anatomies. The CZT detector and the silicon-strip detector differ in energy resolution, charge sharing and pileup effects (see Fig. 1). The CZT detector suffers more from pulse pileup and charge sharing than the silicon-strip detector and has worse energy resolution, whereas the silicon-strip detector yields a higher fraction of Compton scattering. Thus they have distinctive performances in the threshold optimization. For each detector, targets and

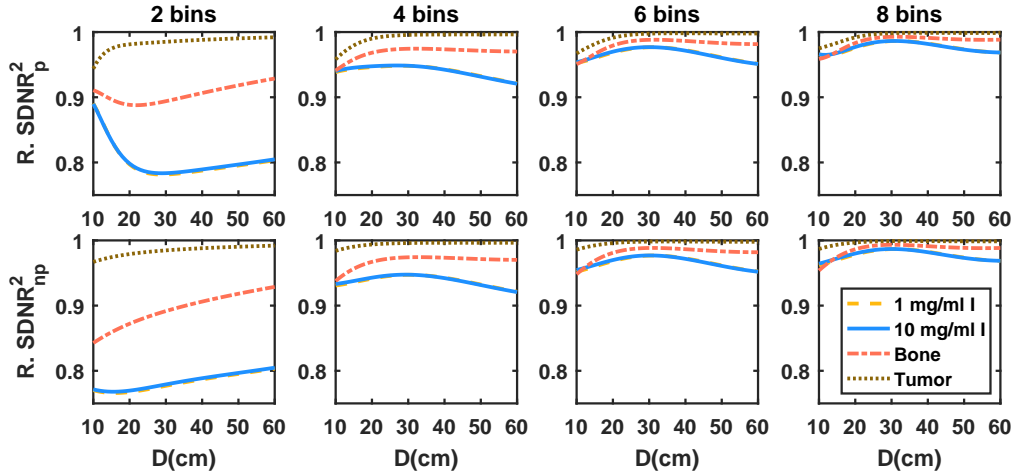


Figure 7: SDNR^2 as a function of phantom thickness and target materials in the silicon-strip detector when thresholds are fixed as the optimal thresholds for phantom 30 cm in Fig. 3. The upper row considers pileup and the lower row neglects pileup.

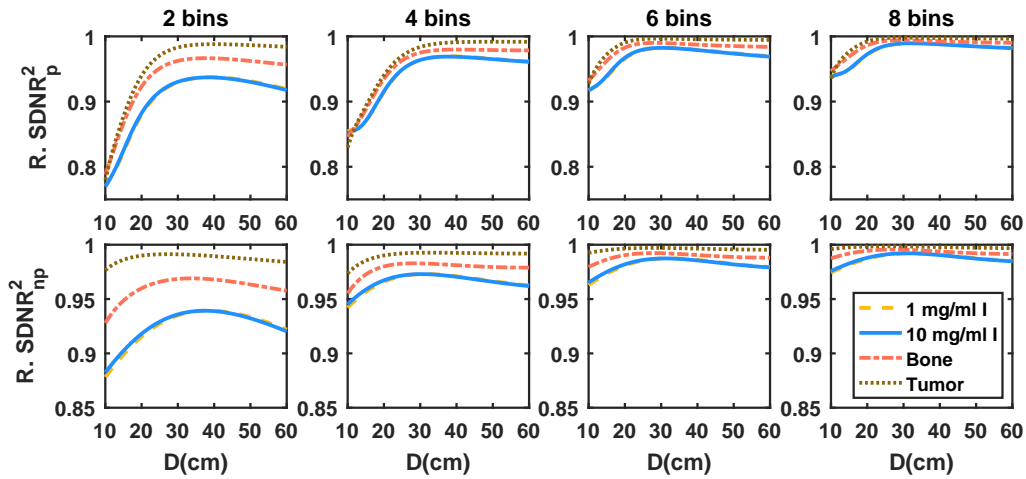


Figure 8: SDNR^2 as a function of phantom thickness and target materials in the CZT detector when thresholds are fixed as the optimal thresholds for phantom 30 cm in Fig. 4. The upper row considers pileup and the lower row neglects pileup.

anatomies are two main influencing parameters in optimizing energy thresholds, and two concerns in examining the robustness of optimal thresholds.

Targets in clinical applications could be iodine contrast agent, tumor, bone, or a mixture of these objects. For both detectors with these targets, the relative optimal SDNR^2 increases with the number of bins (see Fig. 2). For the silicon-strip detector, it's effective to improve optimal SDNR^2 by increasing the number of bins from 2 to 6 or 8 when keeping phantom thickness unchanged. For the CZT detector, on the other hand, the improvement obtained by adding more bins is smaller. Because the CZT detector has deteriorated energy resolution, and a small number of bins are sufficient to capture

the remaining energy information. In Fig. 2, with 2 bins the loss of optimal SDNR^2 reaches 20% in the silicon-strip detector and about 7% in the CZT detector. With 6 to 8 bins, the loss of optimal SDNR^2 is about 1% to 2% in both detectors. When the target is only tumor, setting more bins does not considerably further increase SDNR^2 in both detectors because photons arriving at the detector contain less energy attenuation information. For both detectors, although the relative decrease of optimal SDNR^2 for a threshold error with norm $|\Delta T| = 1$ keV increases with increasing bin numbers, it is still less than 0.4% of the corresponding optimal SDNR^2 (see Fig. 2). It indicates that each optimal SDNR^2 is stable enough to threshold fluctuations regardless of bin numbers. Thus, it is not necessary to set the thresholds with very high precision in applications.

Phantom thickness plays an important role in the threshold optimization because it filters the detected spectrum and changes the fraction of pulse pileup (see Fig. 1). Previous studies have shown that the optimal threshold energies increase with phantom thickness because of the beam hardening effect (Shikhaliyev 2009, Wang & Pelc 2009, Roessl & Proksa 2006, Roessl et al. 2011), which is also demonstrated in Fig. 3 and 4 when pileup is neglected in both detectors. However, with pileup considered, the optimal threshold energies in both detectors don't always increase or even decrease with increasing phantom thicknesses (see Fig. 3 and 4). With a small phantom like 15 cm, pileup is severe and the optimal thresholds lie around 120 keV in Fig. 3 and 4, indicating that the pileup counts above 120 kVp in Fig. 1a contain useful attenuation information. The pileup effect is weakened with a larger and larger phantom because more photons are filtered and less counts pile up. For both detectors, when the phantom is 50 cm, the optimal thresholds considering pileup are nearly the same as those neglecting pileup (see Fig. 3 and 4). In the silicon-strip detector, the optimal threshold energies are not considerably changed by pileup (see Fig. 3) because the output spectrum is not severely distorted by pileup (see Fig. 1). For the CZT detector, the first optimal threshold is always higher than 20 keV regardless of bins in Fig. 4, indicating that charge sharing counts deteriorate SDNR^2 and should be discarded.

In clinical applications, thresholds are set before exposure, with concern over selecting the number of bins and setting the thresholds to yield near-optimal SDNR^2 over various anatomies and target materials. In both detectors the robustness of optimal thresholds is not sensitive to target materials but sensitive to phantom thicknesses (see Fig. 5 to 8). For the silicon-strip detector, setting optimal thresholds for a 30 cm phantom yields the largest mean and minimum SDNR^2 compared with 15 and 50 cm phantoms, and the decrease of SDNR^2 is within 5% with 6 to 8 bins regardless of pileup (see Fig. 5). For the CZT detector, though setting optimal thresholds for a 30 cm phantom still yields the best SDNR^2 regardless of pileup, however, SDNR^2 as a function of phantom thicknesses varies more violently with pileup included and the loss of SDNR^2 with 6 to 8 bins becomes 8%, larger than 4% when pileup is excluded (see Fig. 6). Technically, it's hard to fix one set of thresholds in both detectors in terms of the variation of anatomies when pileup is considered. According to Fig. 5 and 6, if the decrease of SDNR^2 is tolerable, setting thresholds for a 30 cm phantom yields stable

and satisfactory SDNR^2 with 6 to 8 bins in both detectors. For the silicon-strip detector with 2 bins, the lowest threshold is fixed at 5 keV and the only one threshold remains to be optimized (see Fig. 3), and optimizing just one threshold is not enough to get optimal SDNR^2 at a specific thickness (see Fig. 5). And the decrease of relative SDNR^2 from a 10 cm phantom to a 30 cm phantom with 2 bins in Fig. 5 is because the ideal SDNR^2 degrades to pileup more but the absolute SDNR^2 degrades less. Figure 7 and 8 demonstrate the robustness of optimal thresholds for a 30 cm phantom regardless of the variation of target materials. The relative SDNR^2 of bone and tumor is larger than that of iodine in both detectors when using the optimal thresholds for iodine. The plots of 1 mg/ml iodine and 10 mg/ml iodine almost overlap in Fig. 7 and 8, and we have examined that the optimal thresholds for various concentrated iodine within 5 mg/ml to 20 mg/ml are nearly the same.

In the current research, the counts scattered by the phantom are not considered and the pileup counts are treated indiscriminately in calculating SDNR^2 . The challenge of making full use of the pileup counts requires further study. A tradeoff between higher SDNR^2 and less data needs to be considered to select suitable bin numbers. In Fig. 5 and 6, with 2 energy bins, up to 23% of SDNR^2 is lost, indicating that it's better to have more than 2 bins. The more bins, the higher SDNR^2 . Conversely, when SDNR^2 is close to the ideal SDNR^2 , further increasing bin numbers will not improve SDNR^2 considerably but increase the amount of data. Based on that, using around 6 bins in both detectors helps reduce data and retain near-optimal SDNR^2 at the same time.

5. Conclusion

In this work, the placement and robustness of optimal energy thresholds have been studied using SDNR^2 as a FOM in a silicon-strip detector and a CZT detector, factoring in pileup in both detectors and charge sharing in the CZT detector. The CZT detector suffers more from pileup than the silicon-strip detector. Pileup has an important effect on the placement and robustness of optimal thresholds. Setting optimal thresholds for a 30 cm phantom yields near-optimal SDNR^2 in both detectors regardless of target materials and anatomies. With 6 to 8 bins, the loss of SDNR^2 is 5% in the silicon-strip detector and 8% in the CZT detector. With 2 bins, up to 23% of SDNR^2 is lost in both detectors. Having more than 2 bins reduces the need for changing the thresholds depending on materials and anatomies. There is a tradeoff to select bin numbers between higher SDNR^2 and less data with around 6 bins giving near-optimal SDNR^2 without generating unnecessarily large amounts of data.

Acknowledgments

This study was supported by the China Scholarship Council (CSC). Fredrik Grönberg and Mats Persson have financial interests in Prismatic Sensors AB.

References

- Ballabriga R, Alozy J, Blaj G, Campbell M, Fiederle M, Frojdh E, Heijne E, Llopart X, Pichotka M, Procz S et al. 2013 *Journal of Instrumentation* **8**(02), C02016.
- Barrett H H & Myers K J 2013 *Foundations of image science* John Wiley & Sons.
- Bornefalk H 2011 *Medical physics* **38**(11), 6065–6073.
- Bornefalk H & Danielsson M 2010 *Physics in medicine and biology* **55**(7), 1999.
- Chen H, Xu C, Persson M & Danielsson M 2015 *Journal of Medical Imaging* **2**(4), 043504–043504.
- Cormode D P, Roessl E, Thran A, Skajaa T, Gordon R E, Schlomka J P, Fuster V, Fisher E A, Mulder W J, Proksa R et al. 2010 *Radiology* **256**(3), 774–782.
- Knoll G F 2010 *Radiation detection and measurement* John Wiley & Sons.
- Koenig T, Hamann E, Procz S, Ballabriga R, Cecilia A, Zuber M, Llopart X, Campbell M, Fauler A, Baumbach T et al. 2013 *IEEE Transactions on Nuclear Science* **60**(6), 4713–4718.
- Le H Q, Ducote J L & Molloy S 2010 *Medical physics* **37**(3), 1225–1236.
- Liu X, Bornefalk H, Chen H, Danielsson M, Karlsson S, Persson M, Xu C & Huber B 2014 *IEEE Transactions on Nuclear Science* **61**(3), 1099–1105.
- Liu X, Grönberg F, Sjölin M, Karlsson S & Danielsson M 2016 *Nuclear Instruments and Methods in Physics Research Section A: Accelerators, Spectrometers, Detectors and Associated Equipment* **827**, 102–106.
- Liu X, Persson M, Bornefalk H, Karlsson S, Xu C, Danielsson M & Huber B 2015 *Journal of Medical Imaging* **2**(3), 033502–033502.
- Müllner M, Schlattl H, Hoeschen C & Dietrich O 2015 *Physica Medica* **31**(8), 875–881.
- Persson M, Bujila R, Nowik P, Andersson H, Kull L, Andersson J, Bornefalk H & Danielsson M 2016 *Medical physics* **43**(7), 4398–4411.
- Persson M, Huber B, Karlsson S, Liu X, Chen H, Xu C, Yveborg M, Bornefalk H & Danielsson M 2014 *Physics in medicine and biology* **59**(22), 6709.
- Prince J L & Links J M 2006 *Medical imaging signals and systems* Pearson Prentice Hall Upper Saddle River, New Jersey.
- Roessl E, Brendel B, Engel K J, Schlomka J P, Thran A & Proksa R 2011 *IEEE transactions on medical imaging* **30**(9), 1678–1690.
- Roessl E & Proksa R 2006 in ‘Nuclear Science Symposium Conference Record, 2006. IEEE’ Vol. 3 IEEE pp. 1950–1954.
- Roessl E & Proksa R 2007 *Physics in medicine and biology* **52**(15), 4679.
- Schlomka J, Roessl E, Dorscheid R, Dill S, Martens G, Istel T, Bäumer C, Herrmann C, Steadman R, Zeitler G et al. 2008 *Physics in medicine and biology* **53**(15), 4031.
- Schmidt T G 2009 *Medical physics* **36**(7), 3018–3027.
- Shikhaliev P M 2009 *Physics in medicine and biology* **54**(16), 4971.
- W. H. Press, S. A. Teukolsky W T V & Flannery B P n.d.
- Wang A S, Harrison D, Lobastov V & Tkaczyk J E 2011 *Medical physics* **38**(7), 4265–4275.
- Wang A S & Pelc N J 2009 in ‘SPIE Medical Imaging’ International Society for Optics and Photonics pp. 725821–725821.
- Wang A S & Pelc N J 2011 *IEEE transactions on medical imaging* **30**(1), 84–93.
- Xu C, Chen H, Persson M, Karlsson S, Danielsson M, Svensson C & Bornefalk H 2013 *Nuclear Instruments and Methods in Physics Research Section A: Accelerators, Spectrometers, Detectors and Associated Equipment* **715**, 11–17.
- Xu C, Danielsson M & Bornefalk H 2011 *Nuclear Instruments and Methods in Physics Research Section A: Accelerators, Spectrometers, Detectors and Associated Equipment* **648**, S190–S193.